Submitted to the Annals of Applied Statistics

AN ON-LINE SUPPLEMENT TO: A BAYESIAN SPATIOTEMPORAL MODEL FOR RECONSTRUCTING CLIMATE FROM MULTIPLE POLLEN RECORDS

By Lasse Holmström*, Liisa Ilvonen*, Heikki Seppä†, and Siim Veski‡,

*University of Oulu**, *University of Helsinki*† *and Tallinn University of Technology*‡

1. Analysis of the taxon response model. We consider here whether the Gaussian taxon response model described in Section 2.3 of the main paper leads to a reasonable description of how the observed relative abundance of a taxon depends on temperature. We also discuss the extent to which β_j can be interpreted as an optimal taxon temperature and what role the tolerance parameter γ_j plays in this.

Consider a taxon j and temperature x (either modern or past). In a slightly simplified notation, let

$$\lambda_j(x) = \alpha_j \exp\left[-\left(\frac{\beta_j - x}{\gamma_j}\right)^2\right], \quad j = 1, \ldots, l, \tag{S.1}$$

be the Gaussian response function and let $y_j \in [0, 100]$ be the observed relative abundance of taxon j. Here the parameters α_j, β_j and γ_j are thought of as fixed. According to our multinomial likelihood model ((7) in the main paper) y_j has a binomial distribution given the taxon specific probability $p_j(x)$ which determines the probability that an observed pollen grain belongs to taxon j. The probability $p_j(x)$ is itself a component of a Dirichlet random vector whose distribution is determined by the parameters $\lambda_1, \ldots, \lambda_l$ so that, by the properties of the Dirichlet distribution,

$$\mathbb{E}p_j(x) = \frac{\lambda_j(x)}{\sum_{k=1}^{l} \lambda_k(x)}. \tag{S.2}$$

It follows that

$$\mathbb{E}(y_j|x) = \mathbb{E}(\mathbb{E}(y_j|p_j(x)) = \mathbb{E}(100p_j(x)) = 100\frac{\lambda_j(x)}{\sum_{k=1}^{l} \lambda_k(x)}. \tag{S.3}$$

A non-parametric estimate of the regression function $\mathbb{E}(y_j|x)$ can then be obtained from the training set and one can investigate how well it conforms to the parametric model (S.3).

Thus, let $[x_i, y_{ij}]$, $i = 1, \ldots, n$ be the training data where y_{ij} is the observed relative abundance of taxon j at site i with temperature x_i. Let $\hat{f}_j(x)$ be a non-parametric fit to these data, so that

$$\mathbb{E}(y_j|x) \approx \hat{f}_j(x).$$

We check the plausibility of the Gaussian response assumption by investigating how well the approximation

$$\hat{f}_j(x) \approx 100 \frac{\lambda_j(x)}{\sum_{k=1}^{l} \lambda_k(x)}. \tag{S.4}$$

appears to hold for the most important taxa in our data. To check (S.4), posterior mean values are used for the parameters α_j, β_j and γ_j in the right hand side expression although this choice is probably suboptimal when the goal is to make the approximation (S.4) as accurate as possible. In the following we refer to the right side of (S.4) as the "Gaussian response curve" although because of the denominator it in general does not have to resemble the standard Gaussian function but can in fact assume much more general shapes. A standard Gaussian shape can be produced when the denominator $\sum_{k=1}^{l} \lambda_k(x)$ is approximately constant. This may be the case for example when the scaling parameters α_j are approximately equal and the optimal temperatures β_j are uniformly distributed.

The results for the ten most abundant taxa in the combined set of training and core data are shown in Figures S.1 and S.2. Together they account for over 96% of all relative abundances. Note that for clarity of presentation the vertical scales in the panels of these and the subsequent figures are different. In Figure S.1 the response curves are displayed on the training set temperature range [-4.7°C,7.1°C]. The non-parametric fit employed is robust Loess smoothing (Cleveland, 1979). The fits in most cases look rather similar to the curves defined by the Gaussian response curves suggesting that our relative abundance model is plausible. In many cases the distribution of the training data appears to match the left tail of the response curve. This is confirmed by Figure S.2 that shows the response curves for a much larger range of temperatures. For most taxa the optimal temperature ranges suggested by these curves do not seem unreasonable. The response curves for the lakes Raigastvere and Rõuge look similar which is natural because of their close proximity in Estonia. On the other hand, the geographical locations of lakes Arapisto and Flarken are different and their responses also often look different from those of the two Estonian lakes (cf. Figure 5 in the main paper). The response curves of the two multi-core models (SI and

SP) look similar which is consistent with the fact that the corresponding temperature reconstructions also are similar.

The *Betula* (birch) response is nearly linear over a large range of temperatures showing no pronounced maximum within a reasonable temperature interval (Figure S.2). We also note that the non-parametric fit to the training data (Figure S.1) hints at bimodality which is probably due to the presence of both extreme northern and more southern tree types within the same taxon. For *Alnus* (alder), *Corylus* (hazel), *Quercus* (oak), *Ulmus* (elm) and *Tilia* (linden) the optimal temperature (highest taxon probability) suggested by the response curves is clearly above the training set range (Figure S.2). This is not surprising as the training lakes are located in the northern part of their natural ranges. For most reconstructions the maximum relative abundances (determined by the relative sizes of the posterior means of the α_js if the denominator of (S.2) is approximately constant) of these taxa achieved at optimal temperatures are predicted to reach levels well above their share in the training set and core data. However, the estimated maximum taxon probabilities of these five taxa for the lake Arapisto reconstruction are generally lower than for the other three lakes which all are more southern. Again, this is not unexpected considering the modest share of most of these taxa in the Arapisto core (Figure S.13). The optimal temperatures for *Pinus* (pine) and *Picea* (spruce) are reasonably well captured by the optimum observed abundances in the training set. Gramineae (grasses) are widespread in areas of boreal and temperate climate and their natural habitat cover the entire Fennoscandia. The various reconstruction models put its optimal temperature between 2°C and 5°C but the training set (Figure S.1) appears to include warmer sites where Gramineae pollen was observed in greater relative abundance than the overall relative share of this taxon in all data (2%). The abundance of *Carex*-type (sedges) is known to be more related to ecology (mostly open, moist growing sites) than climate. This may explain the rather unstructured response curves that vary greatly between the different lakes.

The posterior distributions of the taxon optimal temperature parameter β_j and the tolerance γ_j are shown in Figures S.3 and S.4. We first note how for the warmer temperature taxa (*Alnus*, *Corylus*, *Quercus*, *Ulmus* and *Tilia*) the posterior β_j's are much higher than their prior values (the red curve). This may be explained by the fact that the prior distribution for β_j, although very wide, is still centered on the optimal value estimated from the training set and the training lake temperatures (mean value 2.6°C) are likely to be considerably lower than many of the past temperatures at the core lakes.

The posterior distributions of the optimal temperature parameter generally differ between the six reconstructions but for a taxon with a well-defined maximum in the Gaussian response curve, the order from lower to higher temperatures in which the optimal values for various reconstructions appear are generally similar in Figures S.2 and S.3. In such cases the optimum suggested by the response curve and the posterior mean of β_j can also be similar, except when the response curve maximum falls at a very high temperature. Note that in such cases (*Corylus*, *Quercus* and *Tilia*) the response curve maximum and the posterior mean of β_j still tend to be similar for the multi-core reconstructions (SI and SP) suggesting one potential benefit of these more complex models if a clearly interpretable role for β_j is desired.

It appears from the above discussion that there is at best only a rough correspondence between the taxon optimal temperature parameter β_j and the optimal temperature suggested by the model, i.e., the temperature at which the response curve (S.3) and consequently the expected taxon relative abundance reaches its highest value. Of course, part of this lack of correspondence can be explained by the fact that the response curves in Figure S.2 in a sense are only particular point estimates of the probability $p_j(x)$ which in our model is in a fact a stochastic process and therefore they should not be considered as accurate representations of actual taxon occurrence probabilities. Still, we believe that the above observations make it quite clear that one should not interpret the parameter β_j as representing a precise optimal taxon temperature. This in fact is a direct consequence of how the temperature response model is designed. The Gaussian functions (S.1) and the associated β_j's are just building blocks of the full relative response model in (S.2) and (S.3) that can assume many other shapes besides a unimodal function centered at β_j. Further, according to Figure S.4, the posterior values of the tolerance parameter γ_j tend to be very large which makes the response function $\lambda_j(x)$ in (S.1) flat and therefore β_j's role as a clear well-defined optimum temperature not very convincing. For example, note how the very large values of γ_j for *Betula* and Flarken's *Pinus* make the corresponding response curves in Figure S.2 useless for finding an optimal temperature.

2. Reference records from Greenland and Scandinavia. The NGRIP Greenland ice core oxygen isotopic profile in Figure S.5 is often used as a reference when Holocene climate is reconstructed for Northern Europe and the North Atlantic region (Andersen et al., 2004). According to this profile, instead of a relatively short time span of a couple of hundred years as suggested by Figure 6 of the main paper, the transition to warmer Holocene

climate has been considerably more gradual. The spatially independent and spatio-temporal reconstructions (Figures 7 and 8) appear to be in better agreement with such a climate history. Similar conclusions can be drawn from Figure S.6 that displays the temperature derived from the Agassiz and Renland ice core records as deviations from the smoothed estimate of present temperature in Greenland (M.Vinther et al., 2009). Further evidence for the gradual onset of warming is provided by the oxygen isotopic profile from Lake Igelsjön located ca. 10 km south of Lake Flarken displayed in Figure S.7 (Hammarlund et al., 2003) and the chironomid-based temperature reconstructions from Norway in Figures S.8 and S.9 (Velle et al., 2005).

3. Alternative reconstructions. The chronology of Lake Rõuge is relatively sparse from 10200 to 9400 BP consisting of dates that are 200 years apart. This may add to the uncertainty in the timing of the onset of early Holocene warming in temperature reconstruction from Lake Rõuge core. We therefore considered also reconstructions where all data for Lake Rõuge before 9400 BP were left out. The reconstruction made independently for Rõuge is shown in Figure S.10 and the spatially independent and spatio-temporal joint reconstructions for all four lakes are shown in Figures S.11 and S.12. In comparison with Figures 7 and 8 of the main paper the reconstructions for Arapisto, Flarken and Raigastvere have not changed much. The most notable difference is the somewhat shaper onset of early Holocene warming especially in the spatio-temporal reconstructions. This is to be expected now that the beginning of warming for all three lakes is almost simultaneous and therefore spatial correlation smooths the differences less. Of course, the confidence intervals for Rõuge increase now rapidly prior to 9400 BP as the reconstruction there is based purely on prior assumptions.

4. The core chronologies. Towards the end of this document are listed the core chronologies from the four lakes used for temperature reconstruction, as well as their union chronology used for spatio-temporal reconstruction. The dates are expressed as years before present, where 'present' is set at AD 1950. A cross marks a union chronology date for which pollen taxon abundances are not available. Thus, for example in the case of Lake Arapisto, the three top-most sediment samples are dated at 0, 278 and 553 years before present, respectively, and so on.

5. Pollen abundances in sediment layers. Figure S.13 after the chronologies displays for each core lake the relative abundances of the ten most common pollen types in the sediment samples. The black silhouette shows the percentage value of each taxon and the yellow silhouette is the

percentage multiplied by 10, which helps visualize the development of the lowest abundances.

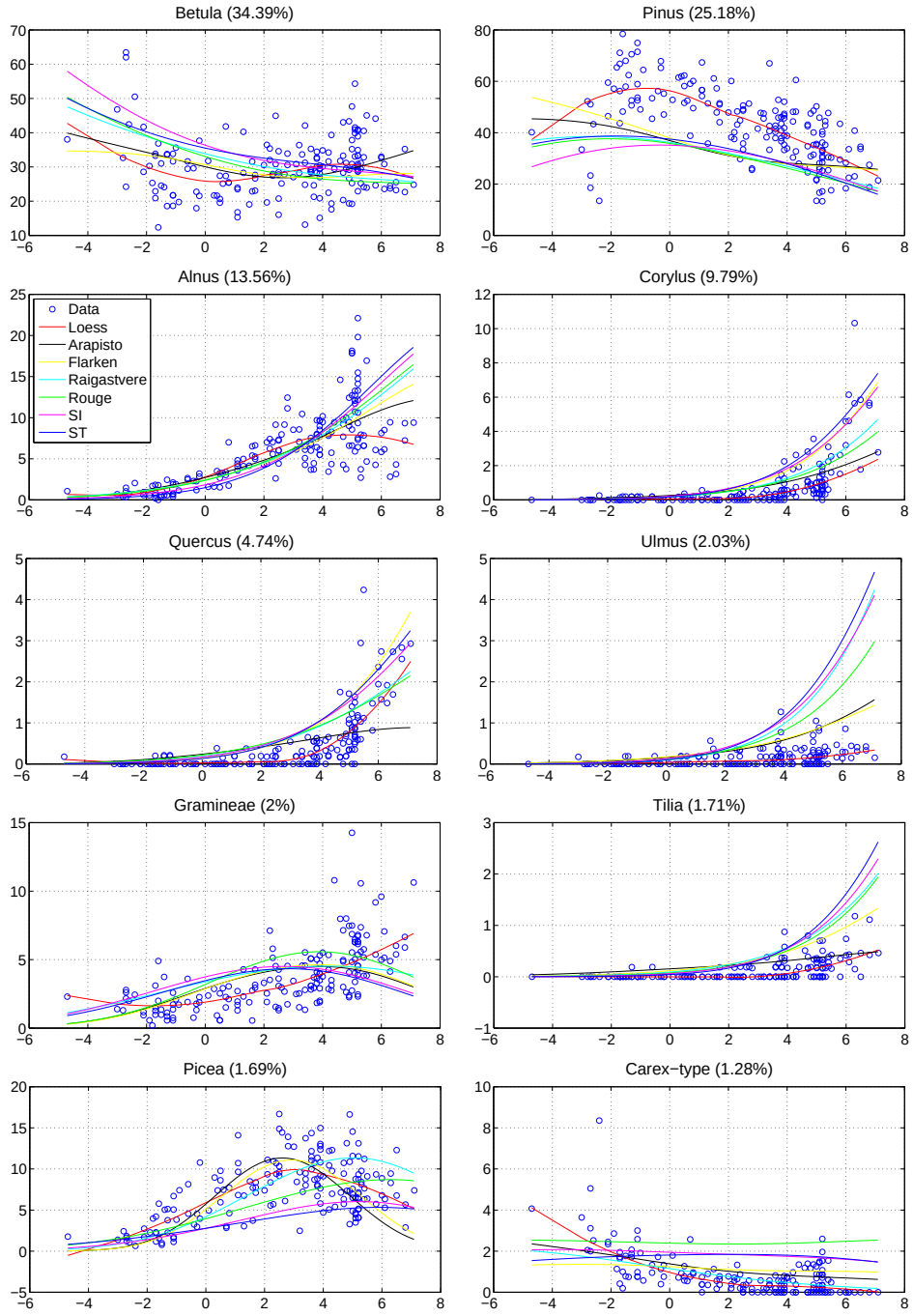

FIGURE S.1. *Checking the plausibility of the Gaussian response model for the ten most abundant taxa. The share of a taxon in all pollen data is shown in the panel title. The legend which is shown only in one instance holds for all panels. The training data are shown as little circles and a non-parametric smooth fitted to them (left side of (S.4)) is shown in red. The other curves correspond to the right side of (S.4) for the various reconstructions: independent reconstruction for each lake, the spatially independent model (SI), and the spatio-temporal model (ST). Horizontal axis is the annual mean temperature (°C).*

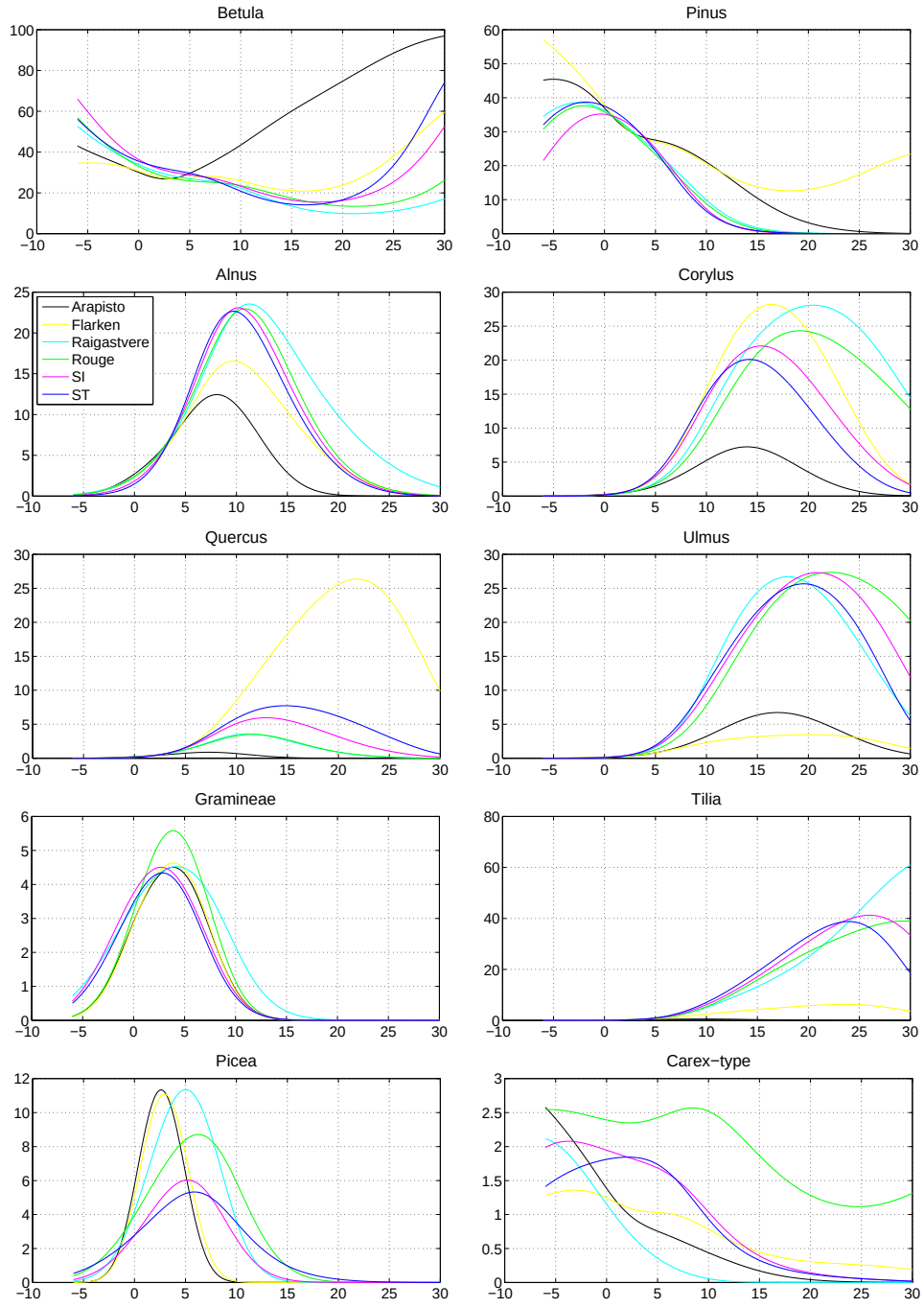

FIGURE S.2. *The Gaussian response model curves of Figure S.1 extended to a wider temperature range.*

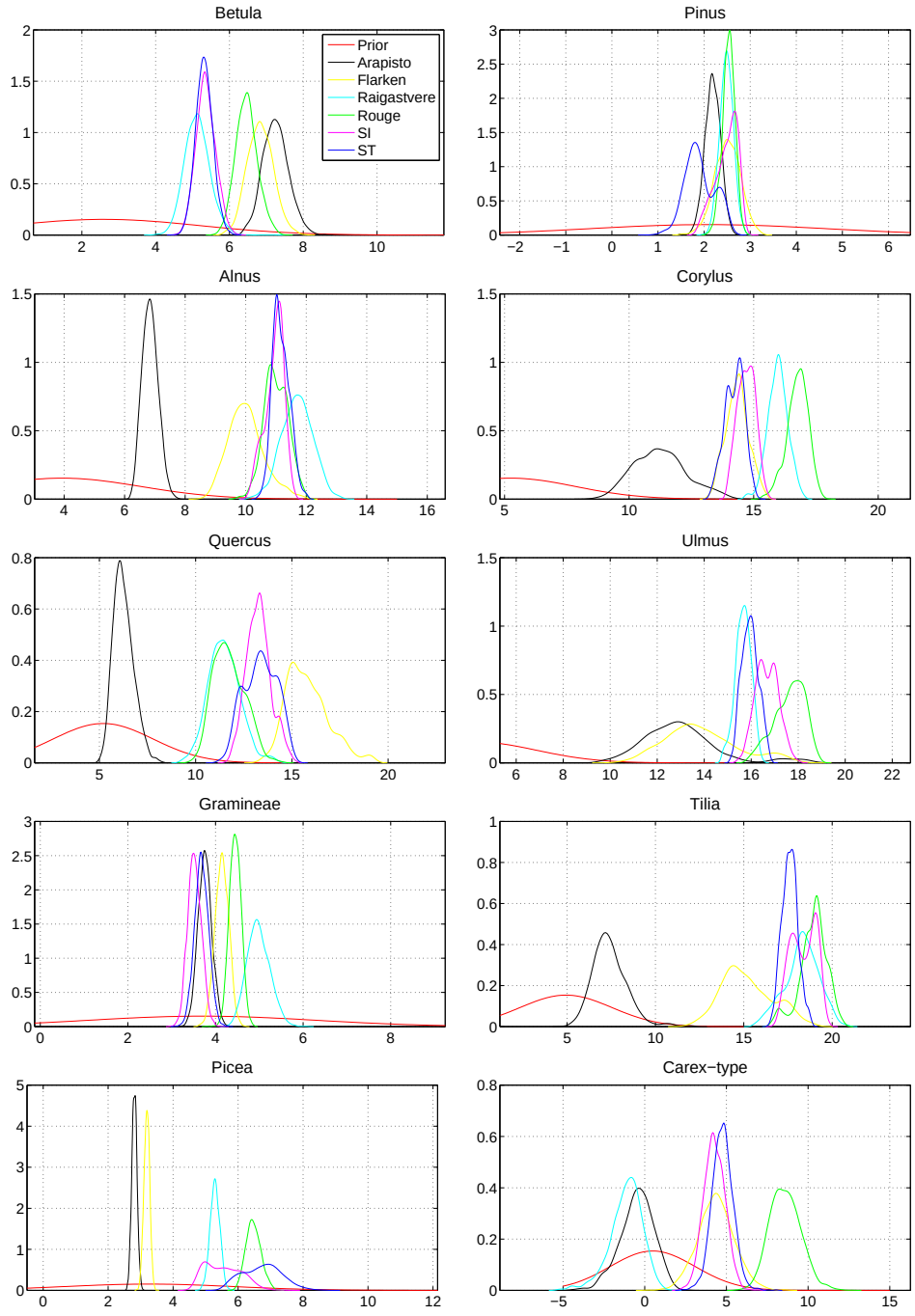

FIGURE S.3. *The posterior distributions of the optimal temperature parameter β_j for the ten most abundant taxa. The colors used for different reconstruction models are indicated in the legend. The prior distribution of β_j (red) is different for each taxon and shows only partially in most panels because each panel focuses on the temperature range where the supports of the posterior distributions are located.*

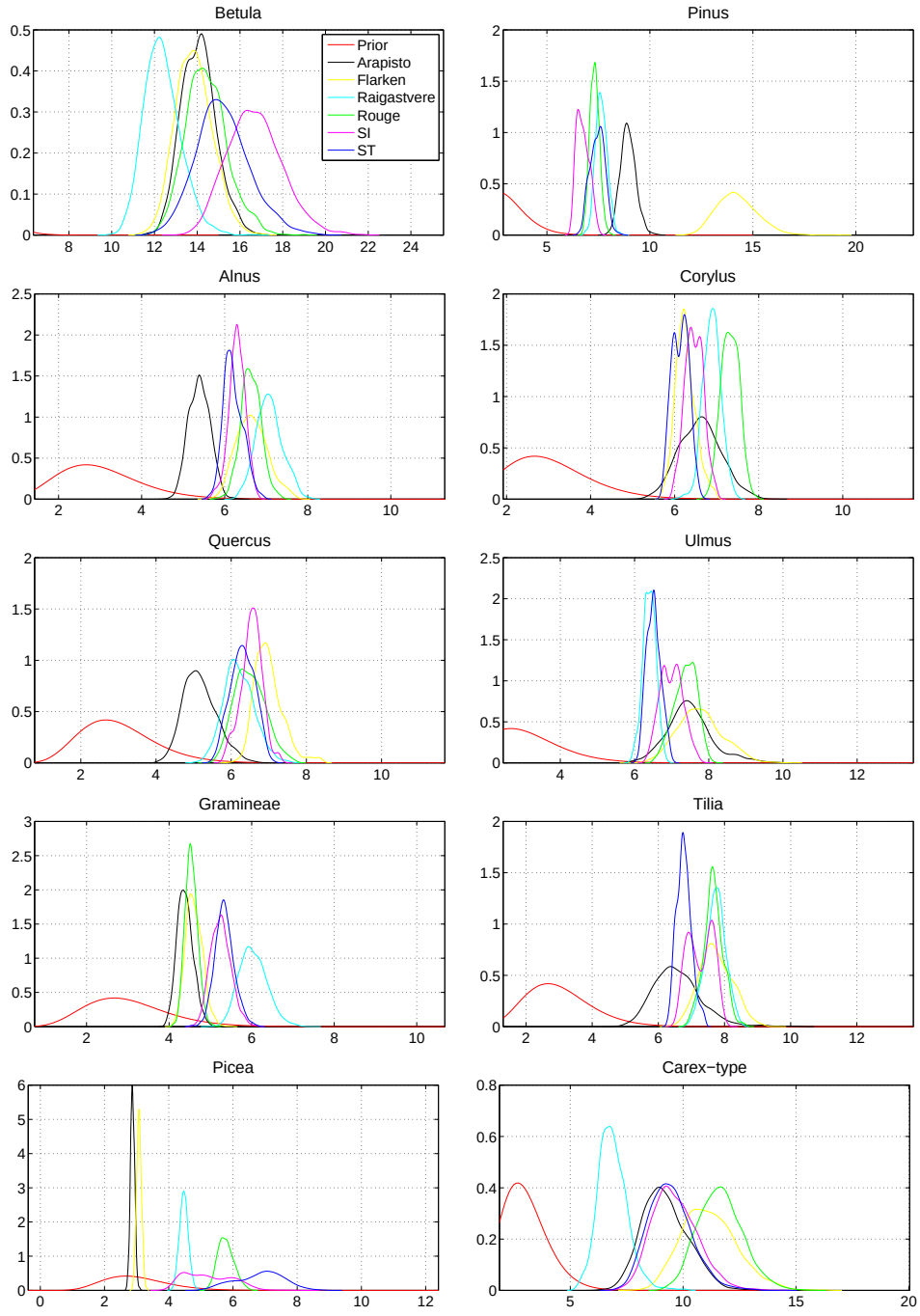

FIGURE S.4. *The posterior distributions of the tolerance parameter γ_j for the ten most abundant taxa. The colors used for different reconstruction models is indicated in the legend. The prior distribution of γ_j (red) is the same for taxa but shows only partially in most panels because each panel focuses on the temperature range where the supports of the posterior distributions are located.*

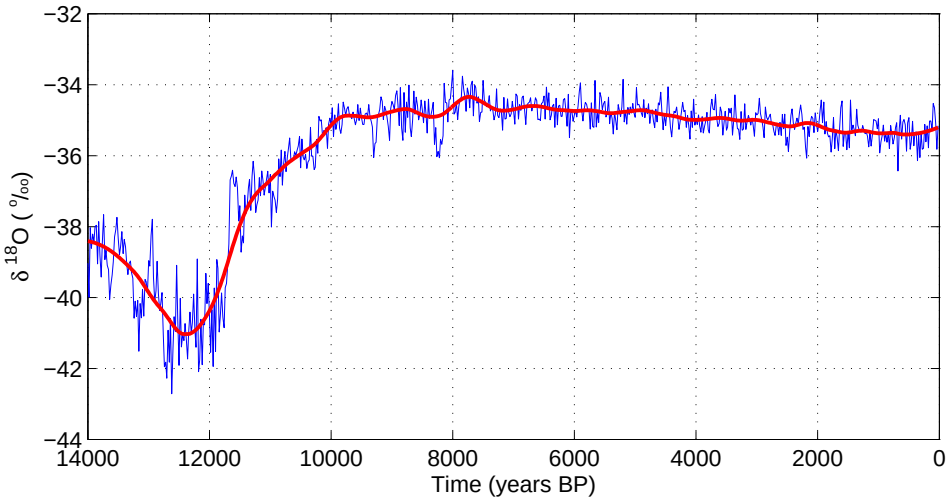

FIGURE S.5. *The Greenland NGRIP oxygen isotopic profile for the last 14000 years. Isotopic values ($\delta^{18}O$) are expressed in permil with respect to Vienna Standard Mean Ocean Water (V-SMOW). The red curve is a robust loess smooth.*

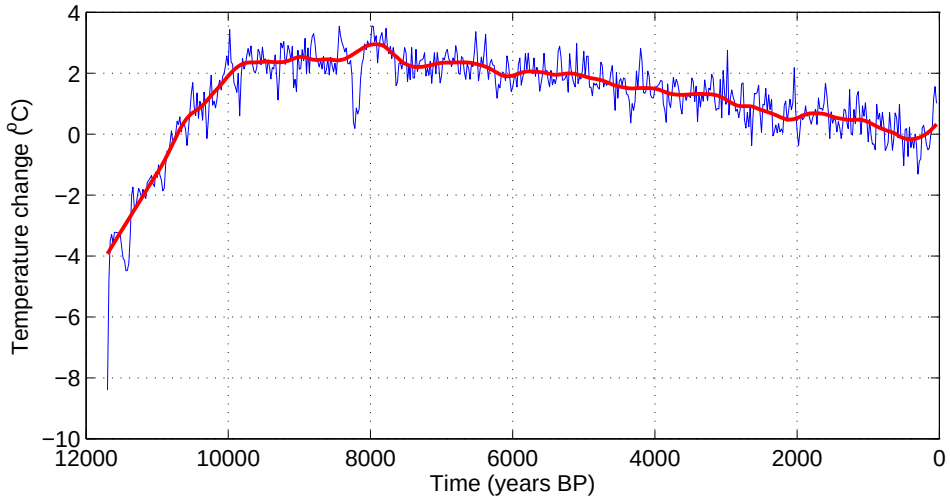

FIGURE S.6. *The temperature for the last 11700 years derived from the Greenland Agassiz and Renland ice core records. The temperature is given as deviations from the smoothed estimate of present temperatures in Greenland. The red curve is a robust loess smooth.*

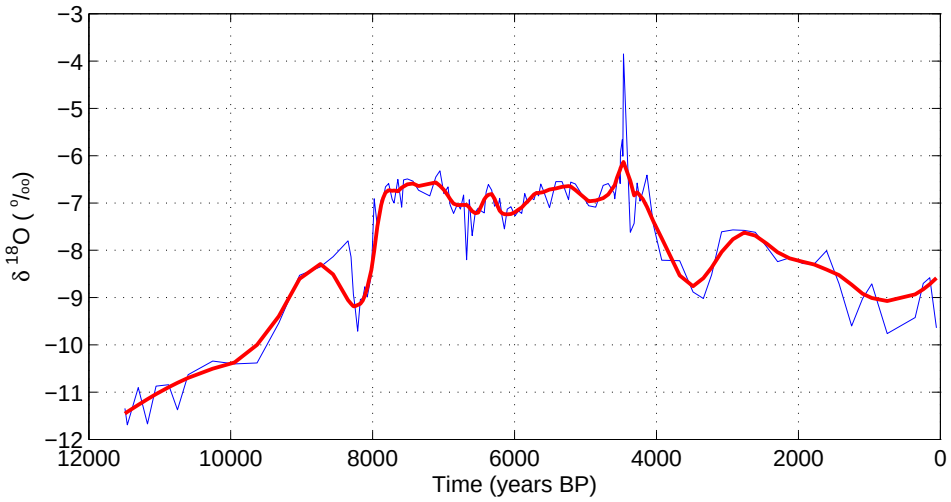

FIGURE S.7. *An oxygen isotopic profile from Lake Igelsjön in south central Sweden (Hammarlund et al., 2003). Isotopic values ($\delta^{18}O$) are expressed in permil with respect to the Vienna Pee Dee Belemnite (V-PDB) standard. The red curve is a robust loess smooth.*

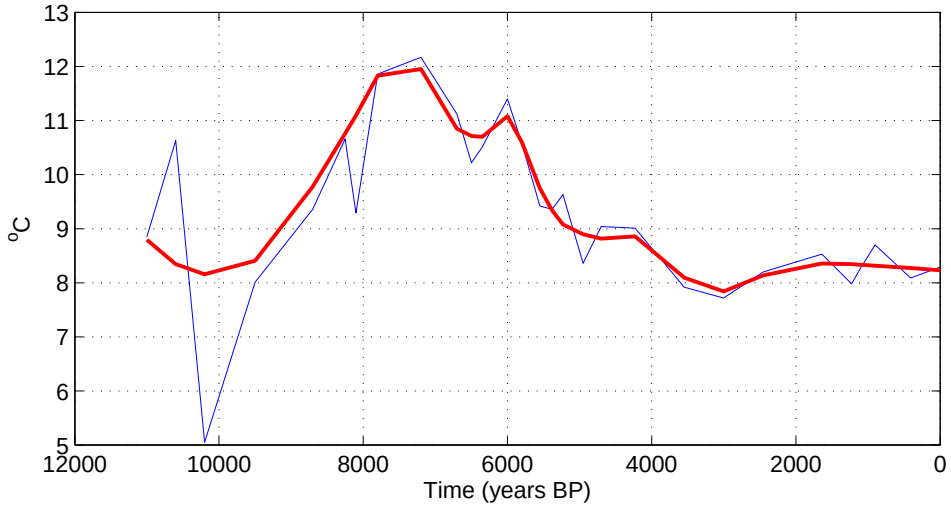

FIGURE S.8. *A chironomid-based temperature reconstruction from Lake Finse Stasjonsdam in mid-southern Norway for the last 11000 years (Velle et al., 2005). The red curve is a robust loess smooth.*

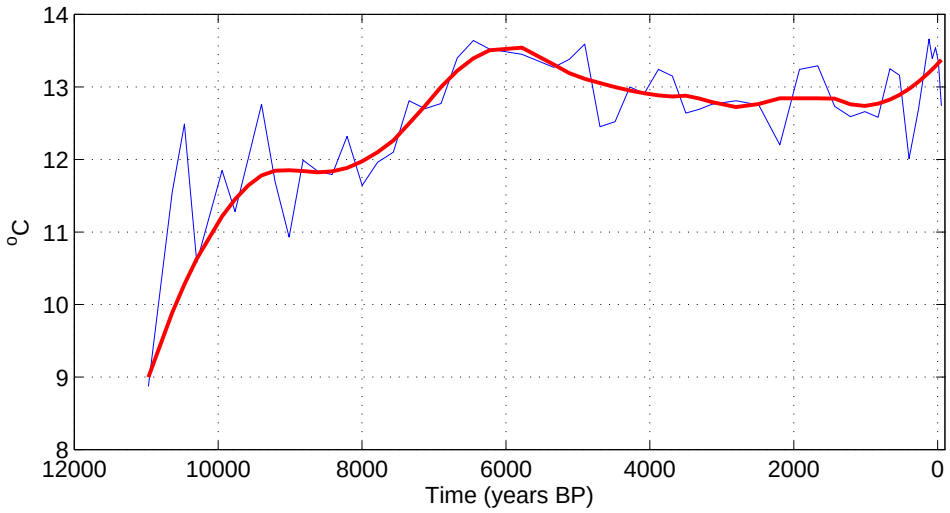

FIGURE S.9. *A chironomid-based temperature reconstruction from Lake Vestre Øyk-jamyrtjørn in southwestern Norway for the last 11000 years (Velle et al., 2005). The red curve is a robust loess smooth.*

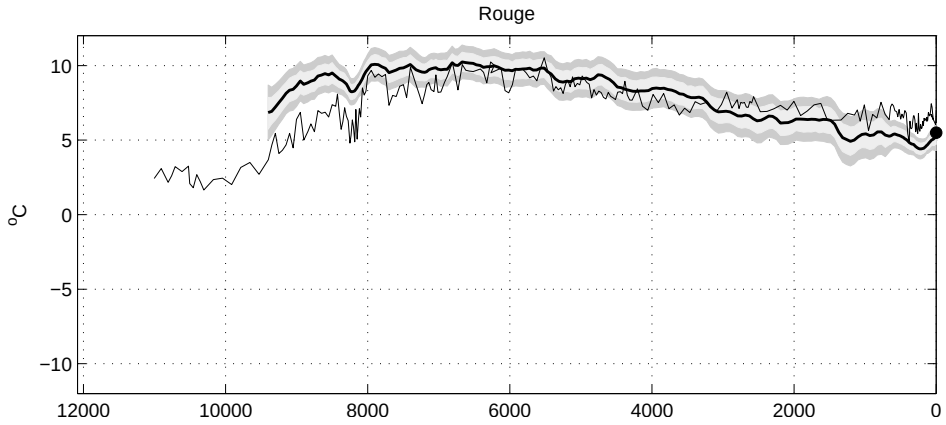

FIGURE S.10. *The temperature reconstruction for Lake Rõuge when all data before 9400 BP have been left out. Light and dark gray show the point-wise and simultaneous 95% credible bands, respectively. Horizontal axis: time in years before present. Vertical axis: mean annual temperature in centigrades. The dot at AD 1950 marks the current mean annual instrumental temperature.*

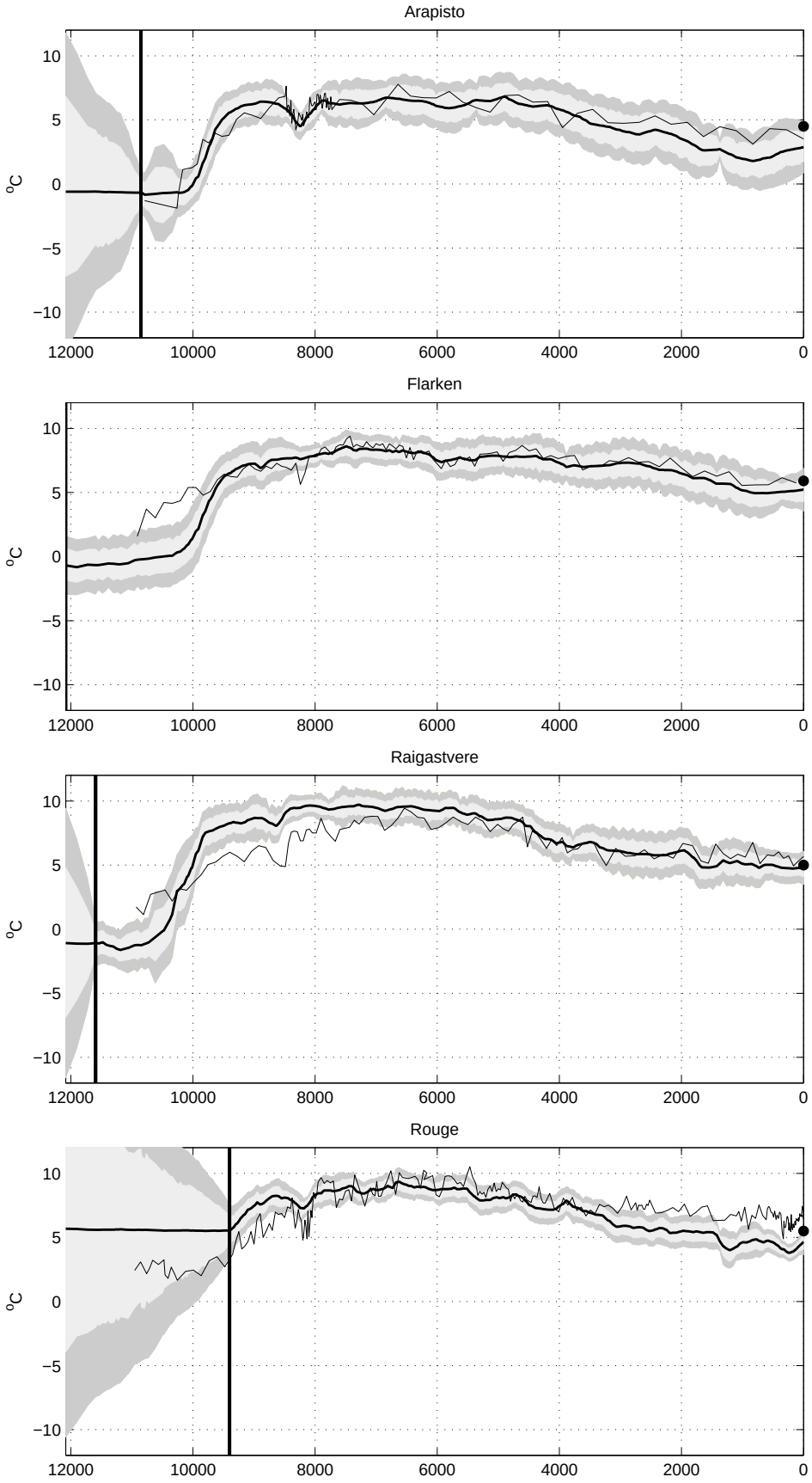

FIGURE S.11. *Temperature reconstructions based on the spatially independent model with no explicit spatial interaction when all data for Lake Rõuge before 9400 BP have been left out. Light and dark gray show the point-wise and simultaneous 95% credible bands, respectively. For each lake, the black line marks the oldest date in its own chronology. Horizontal axis: time in years before present. Vertical axis: mean annual temperature in centigrades. The dot at AD 1950 marks the current mean annual instrumental temperature.*

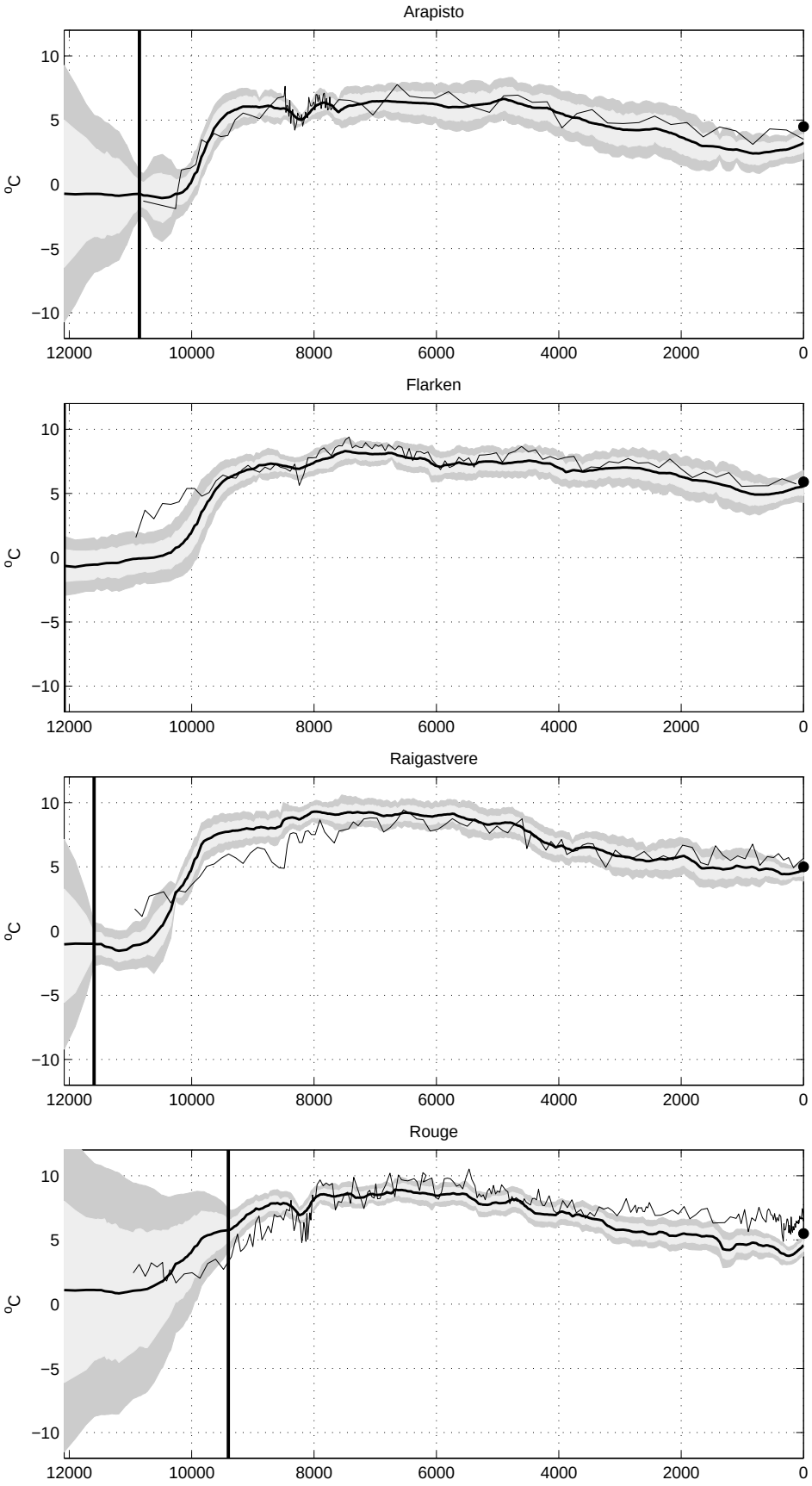

FIGURE S.12. *Temperature reconstructions based on the full spatio-temporal model when all data for Lake Rõuge before 9400 BP have been left out. Light and dark gray show the point-wise and simultaneous 95% credible bands, respectively. For each lake, the black line marks the oldest date in its own chronology. Horizontal axis: time in years before present. Vertical axis: mean annual temperature in centigrades. The dot at AD 1950 marks the current mean annual instrumental temperature.*

References.

Andersen, K. K. et al. (2004). High-resolution record of Northern Hemisphere climate extending into the last interglacial period. *Nature* **431** 147–151.

Cleveland, W. S. (1979). Robust Locally Weighted Regression and Smoothing Scatterplots. *Journal of the American Statistical Association* **74** 829-836.

Hammarlund, D., Bjø"rck, S., Buchardt, B., Israelson, C. and Thomsen, C. T. (2003). Rapid hydrological changes during the Holocene revealed by stable isotope records of lacustrine carbonates from Lake Igelsjön, southern Sweden. *Quaternary Science Reviews* **22** 353 - 370.

Vinther, B. M. et al. (2009). Holocene thinning of the Greenland ice sheet. *Nature* **461** 385–388.

Velle, G., Brooks, S. J., Birks, H. J. B. and Willassen, E. (2005). Chironomids as a tool for inferring Holocene climate: an assessment based on six sites in southern Scandinavia. *Quaternary Science Reviews* **24** 1429 - 1462.

Union	Arapisto	Flarken	Raigast-vere	Rouge
0	0	x	0	0
9	x	x	x	9
29	x	x	x	29
41	x	x	x	41
50	x	x	x	50
59	x	x	x	59
70	x	x	x	70
80	x	x	x	80
86	x	x	86	x
89	x	x	x	89
100	x	x	x	100
111	x	x	x	111
118	x	118	x	x
120	x	x	x	120
129	x	x	x	129
133	x	x	x	133
136	x	x	x	136
150	x	x	x	150
160	x	x	x	160
170	x	x	x	170
172	x	x	172	x
180	x	x	x	180
190	x	x	x	190
200	x	x	x	200
210	x	x	x	210
220	x	x	x	220
230	x	x	x	230
240	x	x	x	240
251	x	x	x	251
259	x	x	259	259
270	x	x	x	270
278	278	x	x	x
280	x	x	x	280
291	x	x	x	291
300	x	x	x	300
311	x	x	x	311
320	x	x	x	320
331	x	x	x	331
341	x	x	x	341
345	x	x	345	x
350	x	350	x	x
352	x	x	x	352

Union	Arapisto	Flarken	Raigast-vere	Rouge
361	x	x	x	361
370	x	x	x	370
380	x	x	x	380
400	x	x	x	400
421	x	x	x	421
431	x	x	431	x
442	x	x	x	442
461	x	x	x	461
483	x	x	x	483
500	x	x	x	500
517	x	x	517	x
522	x	x	x	522
540	x	x	x	540
553	553	x	x	x
557	x	x	x	557
576	x	576	x	x
582	x	x	x	582
602	x	x	x	602
618	x	x	618	x
621	x	x	x	621
641	x	x	x	641
661	x	x	x	661
716	x	x	x	716
734	x	x	734	x
770	x	x	x	770
796	x	796	x	x
825	x	x	x	825
828	828	x	x	x
850	x	x	850	x
880	x	x	x	880
934	x	x	x	934
966	x	x	966	x
989	x	x	x	989
1010	x	1010	x	x
1043	x	x	x	1043
1082	x	x	1082	x
1098	x	x	x	1098
1100	1100	x	x	x
1153	x	x	x	1153
1199	x	x	1199	x
1207	x	x	x	1207
1219	x	1219	x	x

Union	Arapisto	Flarken	Raigast-vere	Rouge
1262	x	x	x	1262
1315	x	x	1315	x
1317	x	x	x	1317
1370	1370	x	x	x
1371	x	x	x	1371
1423	x	1423	x	x
1426	x	x	x	1426
1431	x	x	1431	x
1481	x	x	x	1481
1535	x	x	x	1535
1547	x	x	1547	x
1590	x	x	x	1590
1621	x	1621	x	x
1639	1639	x	x	x
1645	x	x	x	1645
1663	x	x	1663	x
1699	x	x	x	1699
1754	x	x	x	1754
1798	x	x	1798	x
1808	x	x	x	1808
1814	x	1814	x	x
1863	x	x	x	1863
1905	1905	x	x	x
1918	x	x	x	1918
1952	x	x	1952	x
1972	x	x	x	1972
2002	x	2002	x	x
2027	x	x	x	2027
2082	x	x	x	2082
2107	x	x	2107	x
2136	x	x	x	2136
2169	2169	x	x	x
2184	x	2184	x	x
2191	x	x	x	2191
2246	x	x	x	2246
2261	x	x	2261	x
2300	x	x	x	2300
2355	x	x	x	2355
2362	x	2362	x	x
2409	x	x	x	2409
2415	x	x	2415	x
2431	2431	x	x	x

Union	Arapisto	Flarken	Raigast-vere	Rouge
2464	x	x	x	2464
2519	x	x	x	2519
2534	x	2534	x	x
2570	x	x	2570	x
2573	x	x	0	2573
2628	x	x	x	2628
2683	x	x	x	2683
2690	2690	x	x	x
2702	x	2702	x	x
2724	x	x	2724	x
2737	x	x	x	2737
2792	x	x	x	2792
2847	x	x	x	2847
2866	x	2866	x	x
2878	x	x	2878	x
2901	x	x	x	2901
2947	2947	x	x	x
2956	x	x	x	2956
3011	x	x	x	3011
3024	x	3024	x	x
3033	x	x	3033	x
3065	x	x	x	3065
3120	x	x	x	3120
3174	x	x	x	3174
3179	x	3179	x	x
3187	x	x	3187	x
3201	3201	x	x	x
3229	x	x	x	3229
3284	x	x	x	3284
3310	x	x	3310	x
3328	x	3328	x	x
3338	x	x	x	3338
3393	x	x	x	3393
3403	x	x	3403	x
3448	x	x	x	3448
3453	3453	x	x	x
3474	x	3474	x	x
3496	x	x	3496	x
3502	x	x	x	3502
3557	x	x	x	3557
3589	x	x	3589	x
3612	x	x	x	3612

Union	Arapisto	Flarken	Raigast-vere	Rouge
3615	x	3615	x	x
3666	x	x	x	3666
3682	x	x	3682	x
3702	3702	x	x	x
3721	x	x	x	3721
3752	x	3752	x	x
3774	x	x	3774	x
3775	x	x	x	3775
3830	x	x	x	3830
3867	x	x	3867	x
3885	x	x	x	3885
3886	x	3886	x	x
3939	x	x	x	3939
3948	3948	x	x	x
3960	x	x	3960	x
3994	x	x	x	3994
4015	x	4015	x	x
4049	x	x	x	4049
4053	x	x	4053	x
4103	x	x	x	4103
4140	x	4140	x	x
4146	x	x	4146	x
4158	x	x	x	4158
4191	4191	x	x	x
4213	x	x	x	4213
4232	x	x	4232	x
4262	x	4262	x	x
4267	x	x	x	4267
4313	x	x	4313	x
4322	x	x	x	4322
4376	x	x	x	4376
4380	x	4380	x	x
4393	x	x	4393	x
4431	4431	x	x	4431
4473	x	x	4473	x
4486	x	x	x	4486
4495	x	4495	x	x
4540	x	x	x	4540
4553	x	x	4553	x
4595	x	x	x	4595
4606	x	4606	x	x
4634	x	x	4634	x

Union	Arapisto	Flarken	Raigast-vere	Rouge
4650	x	x	x	4650
4667	4667	x	x	x
4704	x	x	x	4704
4714	x	4714	4714	x
4759	x	x	x	4759
4794	x	x	4794	x
4814	x	x	x	4814
4819	x	4819	x	x
4868	x	x	x	4868
4875	x	x	4875	x
4901	4901	x	x	x
4921	x	4921	x	x
4923	x	x	x	4923
4955	x	x	4955	x
4978	x	x	x	4978
5019	x	5019	x	x
5032	x	x	x	5032
5052	x	x	5052	x
5087	x	x	x	5087
5115	x	5115	x	x
5131	5131	x	x	x
5141	x	x	x	5141
5167	x	x	5167	x
5196	x	x	x	5196
5208	x	5208	x	x
5251	x	x	x	5251
5281	x	x	5281	x
5298	x	5298	x	x
5305	x	x	x	5305
5358	5358	x	x	x
5360	x	x	x	5360
5385	x	5385	x	x
5395	x	x	5395	x
5418	x	x	x	5418
5470	x	5470	x	5470
5509	x	x	5509	x
5515	x	x	x	5515
5552	x	5552	x	x
5570	x	x	x	5570
5581	5581	x	x	x
5620	x	x	x	5620
5624	x	x	5624	x

Union	Arapisto	Flarken	Raigast-vere	Rouge
5632	x	5632	x	x
5670	x	x	x	5670
5710	x	5710	x	x
5720	x	x	x	5720
5738	x	x	5738	x
5770	x	x	x	5770
5786	x	5786	x	x
5801	5801	x	x	x
5820	x	x	x	5820
5852	x	x	5852	x
5860	x	5860	x	x
5870	x	x	x	5870
5920	x	x	x	5920
5931	x	5931	x	x
5965	x	x	x	5965
5967	x	x	5967	x
6001	x	6001	x	x
6015	x	x	x	6015
6017	6017	x	x	x
6067	x	x	x	6067
6069	x	6069	x	x
6081	x	x	6081	x
6125	x	x	x	6125
6136	x	6136	x	x
6165	x	x	x	6165
6194	x	x	6194	x
6200	x	6200	x	x
6219	x	x	x	6219
6229	6229	x	x	x
6264	x	6264	x	x
6270	x	x	x	6270
6304	x	x	6304	x
6324	x	x	x	6324
6326	x	6326	x	x
6370	x	x	x	6370
6386	x	6386	x	x
6415	x	x	6415	6415
6437	6437	x	x	x
6446	x	6446	x	x
6470	x	x	x	6470
6504	x	6504	x	x
6516	x	x	x	6516

Union	Arapisto	Flarken	Raigast-vere	Rouge
6526	x	x	6526	x
6562	x	6562	x	x
6570	x	x	x	6570
6619	x	6619	x	x
6620	x	x	x	6620
6637	x	x	6637	x
6641	6641	x	x	x
6670	x	x	x	6670
6674	x	6674	x	x
6729	x	x	x	6729
6730	x	6730	x	x
6748	x	x	6748	x
6770	x	x	x	6770
6784	x	6784	x	x
6809	x	x	x	6809
6838	x	6838	x	x
6841	6841	x	x	x
6859	x	x	6859	x
6880	x	x	x	6880
6892	x	6892	x	x
6920	x	x	x	6920
6945	x	6945	x	x
6970	x	x	6970	6970
6998	x	6998	x	x
7012	x	x	x	7012
7037	7037	x	x	x
7040	x	x	x	7040
7051	x	7051	x	x
7067	x	x	x	7067
7081	x	x	7081	x
7104	x	7104	x	x
7108	x	x	x	7108
7140	x	x	x	7140
7157	x	7157	x	x
7170	x	x	x	7170
7192	x	x	7192	x
7198	x	x	x	7198
7211	x	7211	x	x
7229	7229	x	x	x
7235	x	x	x	7235
7264	x	7264	x	x
7270	x	x	x	7270

Union	Arapisto	Flarken	Raigast-vere	Rouge
7288	x	x	7288	x
7318	x	7318	x	x
7320	x	x	x	7320
7370	x	x	7370	x
7373	x	7373	x	x
7400	x	x	x	7400
7416	7416	x	x	x
7428	x	7428	x	x
7451	x	x	7451	x
7453	x	x	x	7453
7484	x	7484	x	x
7498	x	x	x	7498
7540	x	7540	x	x
7550	x	x	x	7550
7597	x	7597	x	x
7599	7599	x	x	x
7600	x	x	x	7600
7615	x	x	7615	x
7650	x	x	x	7650
7656	x	7656	x	x
7696	x	x	7696	x
7700	x	x	x	7700
7715	x	7715	x	x
7724	7724	x	x	x
7742	7742	x	x	x
7750	x	x	x	7750
7759	7759	x	x	x
7776	x	7776	x	x
7777	7777	x	x	x
7778	x	x	7778	x
7795	7795	x	x	x
7800	x	x	x	7800
7812	7812	x	x	x
7830	7830	x	x	x
7838	x	7838	x	x
7847	7847	x	x	x
7850	x	x	x	7850
7860	x	x	7860	x
7864	7864	x	x	x
7882	7882	x	x	x
7899	7899	x	x	x
7900	x	x	x	7900

Union	Arapisto	Flarken	Raigast-vere	Rouge
7901	x	7901	x	x
7916	7916	x	x	x
7933	7933	x	x	x
7942	x	x	7942	x
7950	x	x	x	7950
7951	7951	x	x	x
7965	x	7965	x	x
7968	7968	x	x	x
7985	7985	x	x	x
8000	x	x	x	8000
8002	8002	x	x	x
8019	8019	x	x	x
8023	x	x	8023	x
8025	x	x	x	8025
8032	x	8032	x	x
8036	8036	x	x	x
8050	x	x	x	8050
8052	8052	x	x	x
8069	8069	x	x	x
8075	x	x	x	8075
8086	8086	x	x	x
8090	x	x	8090	x
8099	x	8099	x	x
8100	x	x	x	8100
8103	8103	x	x	x
8118	x	x	x	8118
8119	8119	x	x	x
8130	x	x	x	8130
8136	8136	x	x	x
8141	x	x	8141	x
8150	x	x	x	8150
8152	8152	x	x	x
8166	x	x	x	8166
8169	8169	8169	x	x
8183	x	x	x	8183
8185	8185	x	x	x
8193	x	x	8193	x
8200	x	x	x	8200
8202	8202	x	x	x
8217	x	x	x	8217
8218	8218	x	x	x
8234	x	x	x	8234

Union	Arapisto	Flarken	Raigast-vere	Rouge
8235	8235	x	x	x
8241	x	8241	x	x
8244	x	x	8244	x
8250	x	x	x	8250
8251	8251	x	x	x
8267	8267	x	x	x
8275	x	x	x	8275
8283	8283	x	x	x
8295	x	x	8295	x
8300	x	x	x	8300
8314	x	8314	x	x
8315	8315	x	x	x
8325	x	x	x	8325
8331	8331	x	x	x
8347	8347	x	8347	x
8350	x	x	x	8350
8363	8363	x	x	x
8375	x	x	x	8375
8379	8379	x	x	x
8389	x	8389	x	x
8395	8395	x	x	x
8398	x	x	8398	x
8400	x	x	x	8400
8411	8411	x	x	x
8425	x	x	x	8425
8427	8427	x	x	x
8442	8442	x	x	x
8450	x	x	8450	8450
8458	8458	x	x	x
8467	x	8467	x	x
8473	8473	x	x	x
8489	8489	x	x	x
8500	x	x	x	8500
8501	x	x	8501	x
8547	x	8547	x	x
8550	x	x	x	8550
8552	x	x	8552	x
8596	8596	x	x	x
8600	x	x	x	8600
8629	x	8629	x	x
8636	x	x	8636	x
8650	x	x	x	8650

Union	Arapisto	Flarken	Raigast-vere	Rouge
8700	x	x	x	8700
8713	x	8713	x	x
8745	8745	x	x	x
8750	x	x	x	8750
8752	x	x	8752	x
8800	x	8800	x	8800
8841	x	x	x	8841
8868	x	x	8868	x
8889	8889	x	x	x
8890	x	8890	x	x
8900	x	x	x	8900
8948	x	x	x	8948
8983	x	8983	x	x
8984	x	x	8984	x
9002	x	x	x	9002
9027	9027	x	x	x
9050	x	x	x	9050
9078	x	9078	x	x
9100	x	x	9100	9100
9148	x	x	x	9148
9160	9160	x	x	x
9176	x	9176	x	x
9200	x	x	x	9200
9216	x	x	9216	x
9250	x	x	x	9250
9277	x	9277	x	x
9287	9287	x	x	x
9300	x	x	x	9300
9332	x	x	9332	x
9350	x	x	x	9350
9381	x	9381	x	x
9400	x	x	x	9400
9409	9409	x	x	x
9448	x	x	9448	x
9489	x	9489	x	x
9525	9525	x	x	x
9564	x	x	9564	x
9600	x	9600	x	9600
9635	9635	x	x	x
9680	x	x	9680	x
9714	x	9714	x	x
9739	9739	x	x	x

Union	Arapisto	Flarken	Raigast-vere	Rouge
9796	x	x	9796	x
9800	x	x	x	9800
9832	x	9832	x	x
9838	9838	x	x	x
9912	x	x	9912	x
9930	9930	x	x	x
9953	x	9953	x	x
10000	x	x	x	10000
10016	10016	x	x	x
10028	x	x	10028	x
10078	x	10078	x	x
10096	10096	x	x	x
10144	x	x	10144	x
10169	10169	x	x	x
10200	x	x	x	10200
10207	x	10207	x	x
10236	10236	x	x	x
10260	x	x	10260	x
10261	10261	x	x	x
10300	x	x	x	10300
10340	x	10340	x	x
10375	x	x	x	10375
10376	x	x	10376	x
10425	x	x	x	10425
10475	x	x	x	10475
10476	x	10476	x	x
10492	x	x	10492	x
10525	x	x	x	10525
10575	x	x	x	10575
10617	x	10617	x	x
10625	x	x	x	10625
10643	x	x	x	10643
10724	x	x	10724	x
10729	x	x	x	10729

Union	Arapisto	Flarken	Raigast-vere	Rouge
10762	x	10762	x	x
10791	10791	x	x	x
10825	x	x	x	10825
10840	x	x	10840	x
10852	10852	x	x	x
10875	x	x	x	10875
10911	x	10911	x	x
10922	x	x	x	10922
10956	x	x	10956	x
11019	x	x	x	11019
11065	x	11065	x	x
11072	x	x	11072	x
11128	x	x	x	11128
11188	x	x	11188	x
11221	x	x	x	11221
11223	x	11223	x	x
11246	x	x	11246	x
11304	x	x	11304	x
11321	x	x	x	11321
11362	x	x	11362	x
11386	x	11386	x	x
11420	x	x	11420	x
11421	x	x	x	11421
11478	x	x	11478	x
11521	x	x	x	11521
11536	x	x	11536	x
11553	x	11553	x	x
11594	x	x	11594	x
11621	x	x	x	11621
11721	x	x	x	11721
11725	x	11725	x	x
11821	x	x	x	11821
11902	x	11902	x	x
12084	x	12084	x	x

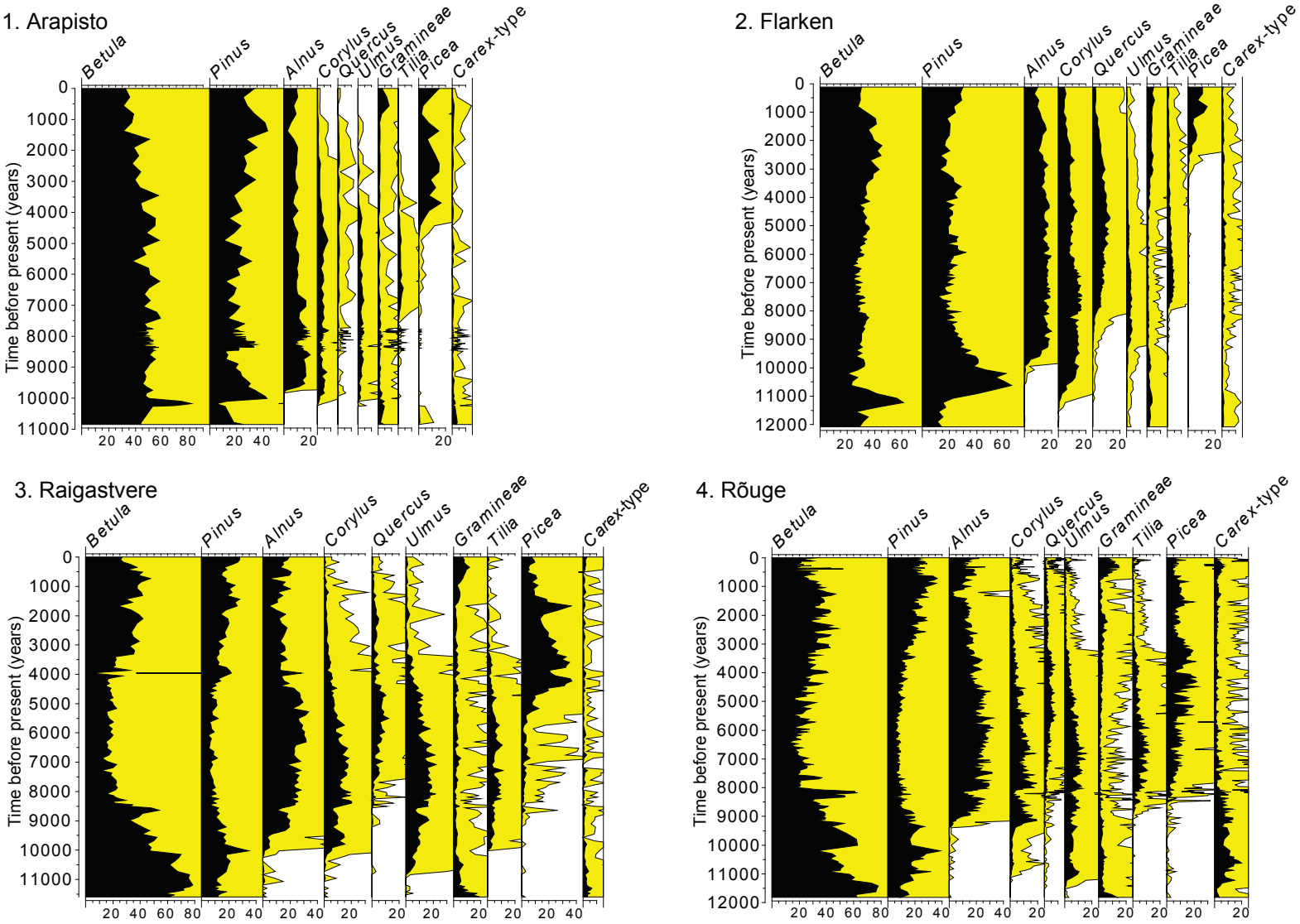

FIGURE S.13. *Pollen diagrams from the four sites for which the temperature reconstructions were made. The diagrams were simplified by showing only the most common pollen types. The black silhouette shows the percentage value of each taxon and the yellow silhouette its 10-fold multiple of abundance.*